

<https://doi.org/10.1038/s42004-025-01503-4>

# Impact of a Terahertz electromagnetic field on the ion permeation of potassium and sodium channels

Zigang Song<sup>1</sup>, Lingfeng Xue<sup>2</sup>, Qi Ouyang<sup>3</sup> & Chen Song<sup>1,2,4</sup>✉

Ion channels are essential for various physiological processes, and their defects are associated with many diseases. Previous research has revealed that a Terahertz electromagnetic field can alter the channel conductance by affecting the motion of chemical groups of ion channels, and hence regulate the electric signals of neurons. In this study, we conducted molecular dynamics simulations to systematically investigate the effects of terahertz electromagnetic fields on the ion permeation of voltage-gated potassium and sodium channels, particularly focusing on the bound ions in the selectivity filters that have not been extensively studied previously. Our results identified multiple new characteristic frequencies and showed that 1.4, 2.2, or 2.9 THz field increases the ion permeability of K<sub>v</sub>1.2, and 2.5 or 48.6 THz field increases the ion permeability of Na<sub>v</sub>1.5. Such effects are specific to the frequencies and directions of the electric field, which are determined by the intrinsic oscillation motions of the permeating ions in the selectivity filter or certain chemical groups of the ion channels. The amplitude of the THz field positively correlates with the change in ion permeation. This study demonstrates that THz fields can specifically regulate ion channel conductances by multiple mechanisms, which may carry great potential in biomedical applications.

Ion channels are integral membrane proteins that control the flow of ions across cellular membranes. They play crucial roles in numerous physiological processes, such as the transmission of neural signals and the initiation of muscle contractions, among other functions. These channels can be categorized on the basis of their ion selectivity, distinguishing them as potassium, sodium, calcium, or chloride channels, or by their gating mechanisms, which include voltage-gated, ligand-gated, and mechanically gated types<sup>1–5</sup>. Dysfunction of ion channels can lead to a variety of diseases, often referred to as channelopathies, including neurological disorders, cardiac arrhythmias, and muscular dystrophies<sup>1</sup>.

Recently, a series of pioneering studies by Chang et al. demonstrated that terahertz (THz, 10<sup>12</sup> Hz) electromagnetic fields can modulate the conductance of various ion channels, thereby influencing neuronal signaling<sup>6–8</sup>. These findings are highly significant and may pave the way for new therapeutic approaches to treating channelopathies. For instance, an experimental study revealed that a 5.6 μm wavelength (53.53 THz) field increased potassium current and modified action potential waveforms<sup>7</sup>. Another study showed that 8.6 μm wavelength (34.88 THz) field improved auditory perception in guinea pigs<sup>9</sup>.

Simulation studies have also indicated that 51.87 THz field can increase ion permeation of the potassium channel KcsA<sup>10,11</sup>, and 53.60 THz field had a similar result on a model K<sup>+</sup> channel<sup>12</sup>. 48.2 THz field was found to increase the ion permeability of sodium channels<sup>13</sup>. 42.55 THz field was found to alter the free energy profile of Ca<sup>2+</sup> in the Ca<sub>v</sub>Ab calcium channel<sup>6</sup>. 36.75 THz field was found to reduce the ion permeability of K<sub>v</sub>1.2 by decreasing the stability of the channel, while the 37.06 THz field had the opposite effect<sup>14</sup>. 15 THz field has been reported to increase the ion permeability by increasing the proportion of direct knock-on permeation<sup>15,16</sup>. A lower frequency of 0.1 THz field was also found to alter the energy profile and accelerate the permeation of K<sup>+</sup> in KcsA<sup>17</sup>. Some other frequencies, such as 1 THz, were also examined<sup>18</sup>. These findings suggest that THz fields may have direct regulation effects on ion channels. Beside ion channels, frequency-specific THz stimulation was also found to enhance surface wettability and induce water flux through artificial channels by energy transfer to water<sup>19,20</sup>. In addition, terahertz waves have been explored for their ability to alter gene expression, detect tumors, and potentially reduce side effects of drugs<sup>21–24</sup>, further demonstrating the therapeutic potential of the THz field.

<sup>1</sup>School of Life Sciences, Peking University, Beijing, China. <sup>2</sup>Center for Quantitative Biology, Academy for Advanced Interdisciplinary Studies, Peking University, Beijing, China. <sup>3</sup>Institute for Advanced Study in Physics, Zhejiang University, Hangzhou, China. <sup>4</sup>Peking-Tsinghua Center for Life Sciences, Academy for Advanced Interdisciplinary Studies, Peking University, Beijing, China. ✉e-mail: [c.song@pku.edu.cn](mailto:c.song@pku.edu.cn)

Although the effects of THz fields on ion channels have been gradually recognized, most of the previous studies focused on the effects of THz fields on certain chemical groups of ion channels. Considering that there are usually well-defined ion binding sites within the selectivity filter (SF) of ion channels, one would expect that these bound ions should have well-defined oscillation motions, and the impact of THz fields on such motions remains largely uninvestigated. Therefore, this study aims to identify previously unknown frequencies that influence ion channel conductance, with a particular focus on those that directly affect the bound ions at the SF of ion channels.

We examined the structure and function of two well-studied ion channels: the voltage-gated potassium channel ( $K_v$ ) and the voltage-gated sodium channel ( $Na_v$ ). The  $K_v$  channel is a tetramer with each subunit featuring an N-terminal domain, six transmembrane helices (S1 ~ S6) and a C-terminal domain. The voltage-sensing domain (VSD) is formed by S1 ~ S4, while S5, S6, and the intervening pore loop constitute the pore region. The SF, which controls the selectivity to ions, locates within the pore loop. It has a characteristic sequence TVGYGD, and provides five binding sites for  $K^+$  ions, named S0 ~ S4. The lower part of S6 helices form the gate, which undergoes conformational changes between different states<sup>1,3-5,25-28</sup>. The structure of a chimeric protein,  $K_v1.2/2.1$  (PDB: 2R9R), resolved in 2007, has been extensively studied and serves as a basis for our open-state  $K_v1.2$  model<sup>29-33</sup> (Fig. 1A).

The eukaryotic  $Na_v$  channel comprises an  $\alpha$  subunit with four similar domains (DI ~ DIV), each containing six transmembrane helices (S1 ~ S6), along with several auxiliary  $\beta$  subunits. The SF is located at the pore loop

between S5 and S6, formed by DEKA and EEDD residues from four domains, and the gate is formed by the lower part of S6 helices<sup>1,2,34-42</sup>.  $Na_v1.5$  is a sodium channel expressed in cardiac muscle and encoded by *SCN5A*<sup>43,44</sup>, whose partially-open structure was solved in 2021 (PDB: 7FBS)<sup>41</sup>. A recent study by Choudhury et al. proposed that the channel fully opens when the S6 helices in domains DI, DIII, and DIV or all four domains form partial  $\pi$ -helices<sup>45</sup>. Therefore, the  $Na_v1.5$  structure model with four manually-introduced  $\pi$  helices was used for this study (Fig. 1B).

In this study, we performed molecular dynamics (MD) simulations to investigate the oscillation motions of bound ions in the SF of  $K_v1.2$  and  $Na_v1.5$ , as well as the effects of THz frequencies on the  $K_v1.2$  and  $Na_v1.5$  channels. Our findings revealed that THz waves with specific frequencies, 1.4, 2.2, and 2.9 THz, enhanced the ion permeation of  $K_v1.2$ , and 2.5 THz field enhanced that of  $Na_v1.5$ , by directly affecting the motion of  $K^+$  or  $Na^+$  bound at the SF of the channels. 48.6 THz field increased the ion permeation of  $Na_v1.5$  by affecting the carboxyl groups ( $-COO^-$ ) at the SF. Conversely, 10.8 THz field decreased ion permeability of  $K_v1.2$  by altering ion distribution. These results further suggest that THz fields could potentially be harnessed for therapeutic applications, offering a novel avenue for manipulating ion channel function.

## Results

### Structural analysis

We first computed the pore radius of each ion channel using HOLE<sup>46</sup> after equilibration to confirm that they adopt a stably open state (Fig. 1 right panels). The pore radius of  $K_v1.2$  was 0.60 Å at SF and 2.90 Å at the gate. The

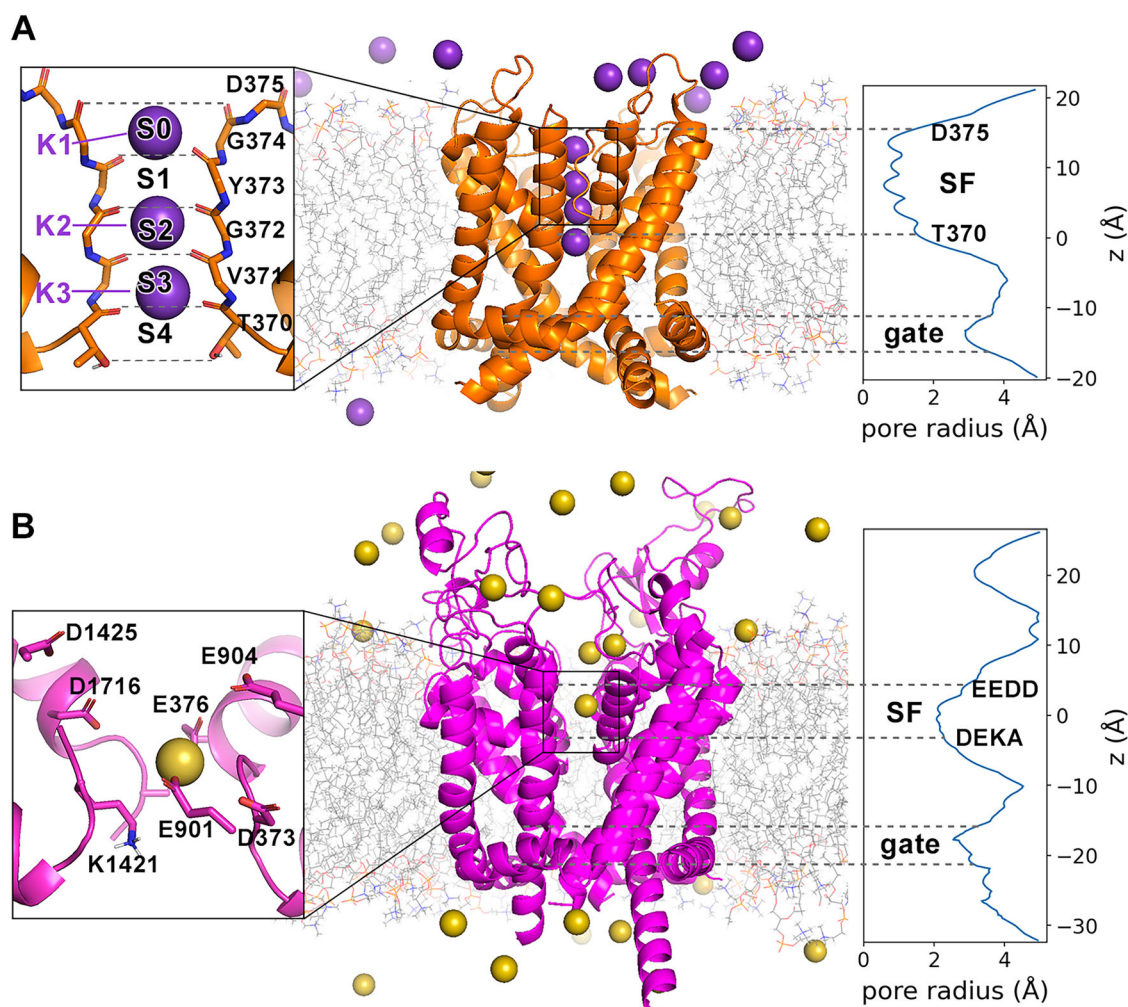


**Fig. 1 | The simulation systems.** (A)  $K_v1.2$ , (B)  $Na_v1.5$ . Purple and yellow spheres represent  $K^+$  and  $Na^+$ , respectively. Each left panel shows the structure of the selectivity filter with the bound ions, and each right panel shows the pore radius along the  $z$ -axis.

pore radius of Na<sub>v</sub>1.5 was 2.07 Å at SF and 2.55 Å at the gate. Both channel models were in their open state, and the SF was the narrowest location in the path of ion permeation.

### Frequency analysis

To identify potential frequencies that influence the motion of the ions within the channels, we performed a frequency analysis using Fast Fourier Transform (FFT) on the trajectories of ions and the atoms or chemical groups that form the ion binding sites within the selectivity filter. This analysis encompassed a frequency range from 0.1 to 100 THz. The ions remained at the binding sites throughout the simulation (Fig. S1). In the following paragraphs, the z direction is perpendicular to the membrane and parallel to the channel, and the x/y directions are parallel to the membrane.

Our findings identified distinct characteristic frequencies for both ions and the key atoms or chemical groups within the channels. In the case of the potassium channel K<sub>v</sub>1.2, three potassium ions occupied the SF after equilibration, binding to S0, S2 and S3/S4 (designated as K1 to K3 respectively). They exhibited vibrational motions predominantly within the 1 to 6 THz range. Specifically, the peak frequencies for these ions in the z direction were 2.2, 2.9, and 1.4 THz, respectively, while their peak frequencies in the x or y directions were approximately 5.0 THz (Fig. 2A).

Additionally, we analyzed the carbonyl oxygen atoms of residues 370 to 375 in K<sub>v</sub>1.2, which form the ion binding sites. We also performed FFT on the bond, angles and dihedrals that the oxygen atoms involve, so as to identify the vibrational modes. The atoms showed a peak frequency of 51.0 THz, corresponding to the stretching vibration mode of the C=O bond, which has been examined in the previous studies<sup>10–12</sup>. Another peak was observed at 10.8 THz in z direction, which mainly resulted from the CA-C-O angle vibration. A third peak at around 3.9 THz in the x-y plane was the

result of N-CA-C-O and CA<sup>+</sup>-N<sup>+</sup>-C-O dihedrals (+1 denotes the atoms from the next residue) (Fig. 2B, Figure S2).

For the sodium channel Na<sub>v</sub>1.5, the Na<sup>+</sup> ion within the SF exhibited a broad frequency spectrum ranging from 1 to 12 THz. A prominent peak at 2.5 THz was associated with the ion's motion in the x-z plane within the SF, while a smaller peak at 10.0 THz corresponded to motion in the y-z plane (Fig. 2C), showing a similar pattern as observed by Zhu et al.<sup>47</sup>.

We also computed the carboxyl groups of Glu and Asp residues that interact with Na<sup>+</sup> ions at the SF (residues 373, 376, 901, 904, 1425, and 1716). These groups exhibited peak frequencies at 48.6 THz and 42.5 THz, both linked to the stretching mode of the C-O bond. The 48.6 THz mode predominantly occurred in the x-z plane, while the 42.5 THz mode was observed in the x-y plane. A third peak showed up at around 2.8 THz, close to the peak frequency of the Na<sup>+</sup> ion (Fig. 2D).

### The effect of THz electromagnetic field

We initially performed control experiments without applying THz fields to establish a baseline for ion permeation, measured by the channel conductance. The conductance was calculated by counting the number of ions passing through the channels over a specified time under certain trans-membrane potentials.

For K<sub>v</sub>1.2, the simulated conductance was  $12.6 \pm 3.2$  picosiemens (pS), consistent with the experimental range of 14 to 18 pS<sup>25</sup>. Throughout these simulations, ions permeated stably through the channel, with an average of three ions occupying the SF.

The simulated conductance of Na<sub>v</sub>1.5 was  $39.1 \pm 12.3$  pS, exceeding but close to the experimental range of 10 to 20 pS<sup>41,48</sup>. This discrepancy may be due to the use of a more open structure in our simulations. Despite the elevated conductance, ion permeation through Na<sub>v</sub>1.5 remained stable, with

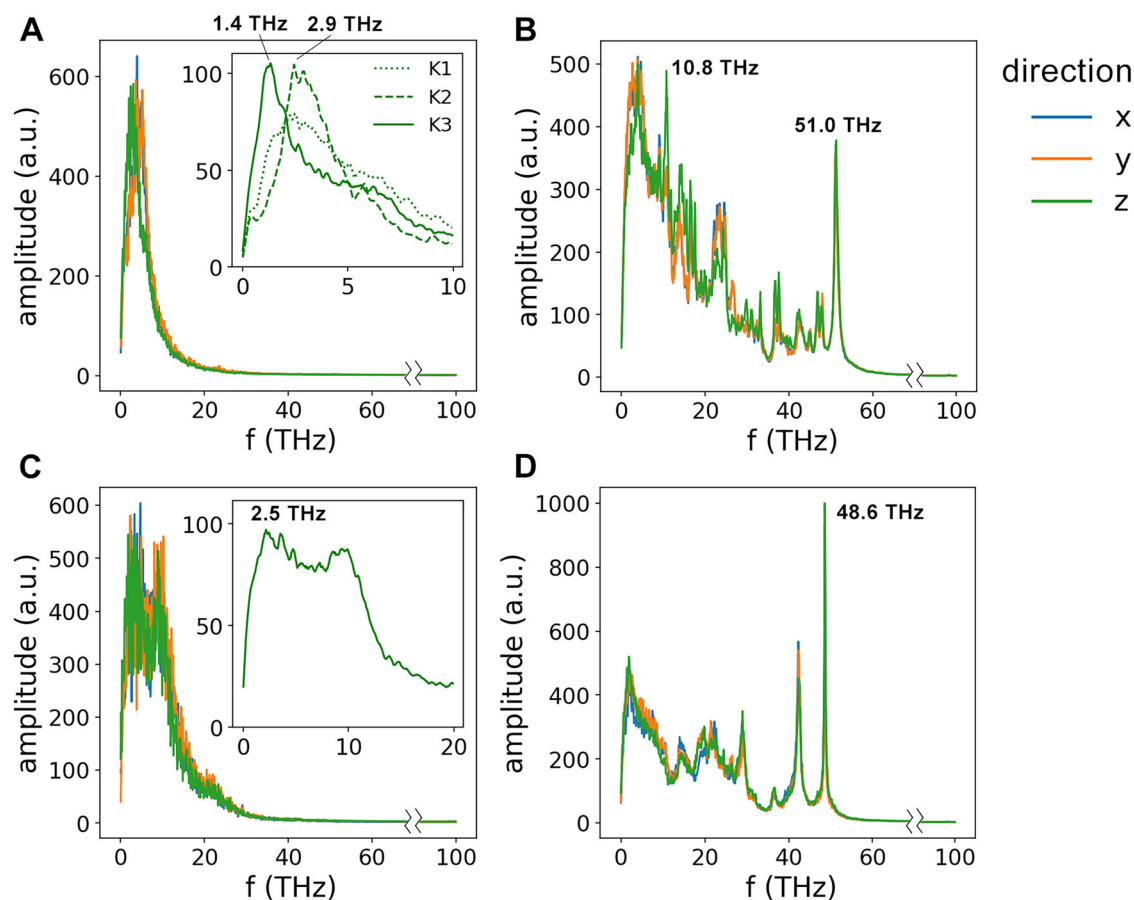


**Fig. 2 | Frequency spectra.** Frequency spectra of (A) K<sup>+</sup> ions within K<sub>v</sub>1.2, with the inset showing the z-direction spectrum of the three individual ions. (B) Oxygen atoms at the selectivity filter (SF) of K<sub>v</sub>1.2. (C) Na<sup>+</sup> ion within Na<sub>v</sub>1.5, with the inset displaying its z-direction spectrum. (D) Carboxyl (-COO) groups at the SF of Na<sub>v</sub>1.5.

an average of one sodium ion occupying the SF during the simulation period.

Subsequently, we applied electromagnetic fields at the observed frequencies to each ion channel system with the focus on the z-direction frequencies, as they are more likely to affect ion permeation<sup>11</sup>. The THz field was applied in the z direction with an amplitude of 0.8 V/nm, and channel conductance was measured under each condition. To determine whether the THz field had a direct impact on the motion of ions, we calculated the difference in average kinetic energy ( $\Delta E_k$ ) of the ions located at SF compared with ions outside the channel (i.e. in the solution). The trajectories were split into 50 ns intervals, and the kinetic energy was averaged within each interval to reduce fluctuations. Additionally, we computed the ion distribution and potential of mean force (PMF) along z axis to determine whether the observed effects were associated with changes in ion distribution and PMF.

**1.4, 2.2 and 2.9 THz fields increased ion permeation of  $K_v1.2$ .** For  $K_v1.2$ , applying electromagnetic fields at frequencies of 1.4, 2.2, and 2.9 THz significantly increased channel conductance to  $31.4 \pm 6.6$ ,  $27.2 \pm 6.5$ , and  $30.8 \pm 9.3$  pS, respectively ( $n = 6$  per frequency,  $p < 0.01$ ). The effects were similar across these frequencies probably due to their proximity, with the 1.4 THz field producing the highest conductance, representing a 2.5-fold increase (Fig. 3A, B). A significant increase in the kinetic energy of the ions was observed ( $1.16 \pm 0.06$ ,  $2.24 \pm 0.17$ , and  $1.33 \pm 0.17$  kJ/mol respectively), indicating that the THz field indeed enhanced ion permeation by directly affecting the ions (Fig. 3C). We noticed that 2.2 THz field yielded the largest  $\Delta E_k$ , but had no advantage over 1.4 or 2.9 THz on ion permeation. Since 2.2 THz corresponds to the vibration in S0, which locates near the surface of the channel, one likely reason is that it is less obstructed and easier to absorb energy.

**10.8 THz field hindered ion permeation in  $K_v1.2$  by altering ion distribution.** In contrast, a 10.8 THz field decreased the conductance to

$3.0 \pm 1.0$  pS ( $n = 3$ ,  $p < 0.01$ ), approximately one-quarter of the original value (Fig. 3A, B). No significant changes in ion distribution were observed with the 1.4, 2.2, or 2.9 THz fields. However, the application of a 10.8 THz field altered the ion distribution and PMF. The occupation state of  $K^+$  shifted to S1, S2/S3, and S4, as opposed to S0, S2 and S3/S4 without the THz field (Fig. 4A, B). By examining the Fourier coefficient of each atom at SF, we noticed that the O atom in residues 370, 371, and 373 were the main contributors to this vibrational mode. The O atom in residue 370 and 371 altered the energy barrier between S2/S3 and S3/S4, and the O atom in residue 373 changed the preferable binding site of K1 from S0 to S1. Therefore, it is likely that this alteration led to the decrease in ion permeation.

**2.5 and 48.6 THz field increased ion permeation of  $Na_v1.5$ .** For  $Na_v1.5$ , the application of a 2.5 THz electromagnetic field dramatically reduced the residence time of  $Na^+$  ions and increased channel conductance to  $133.5 \pm 61.8$  pS ( $n = 6$ ,  $p < 0.05$ ), representing a 3.4-fold increase compared to control conditions (Fig. 3D, E). A  $\Delta E_k$  of  $0.81 \pm 0.19$  kJ/mol was observed, indicating that the THz field directly affects the motion of  $Na^+$  (Fig. 3F). In contrast, applying a 10.0 THz field resulted in an unaffected conductance at  $39.7 \pm 12.6$  pS, although it induced an even higher  $\Delta E_k$  of  $2.18 \pm 0.77$  kJ/mol. This indicates that the kinetic energy was not the sole reason for the increase in ion permeation.

The 48.6 THz field also enhanced ion permeation, but this effect was preceded by a 140 ns low-permeability delay period. Given that a brief 140 ns is significantly shorter than most physiological processes, this was considered as a transient effect. Therefore, we extended the simulation to 600 ns, and analyzed the trajectory after 140 ns when ion permeation became stable (Figure S3). The conductance increased to  $93.0 \pm 22.6$  pS ( $n = 4$ ,  $p < 0.05$ ). The  $Na^+$  ions at the SF exhibited a  $\Delta E_k$  of  $1.14 \pm 0.30$  kJ/mol, which affirms that the motion of carboxyl groups can absorb and transfer the energy to  $Na^+$ , as proposed by Zhao et al.<sup>13</sup>.

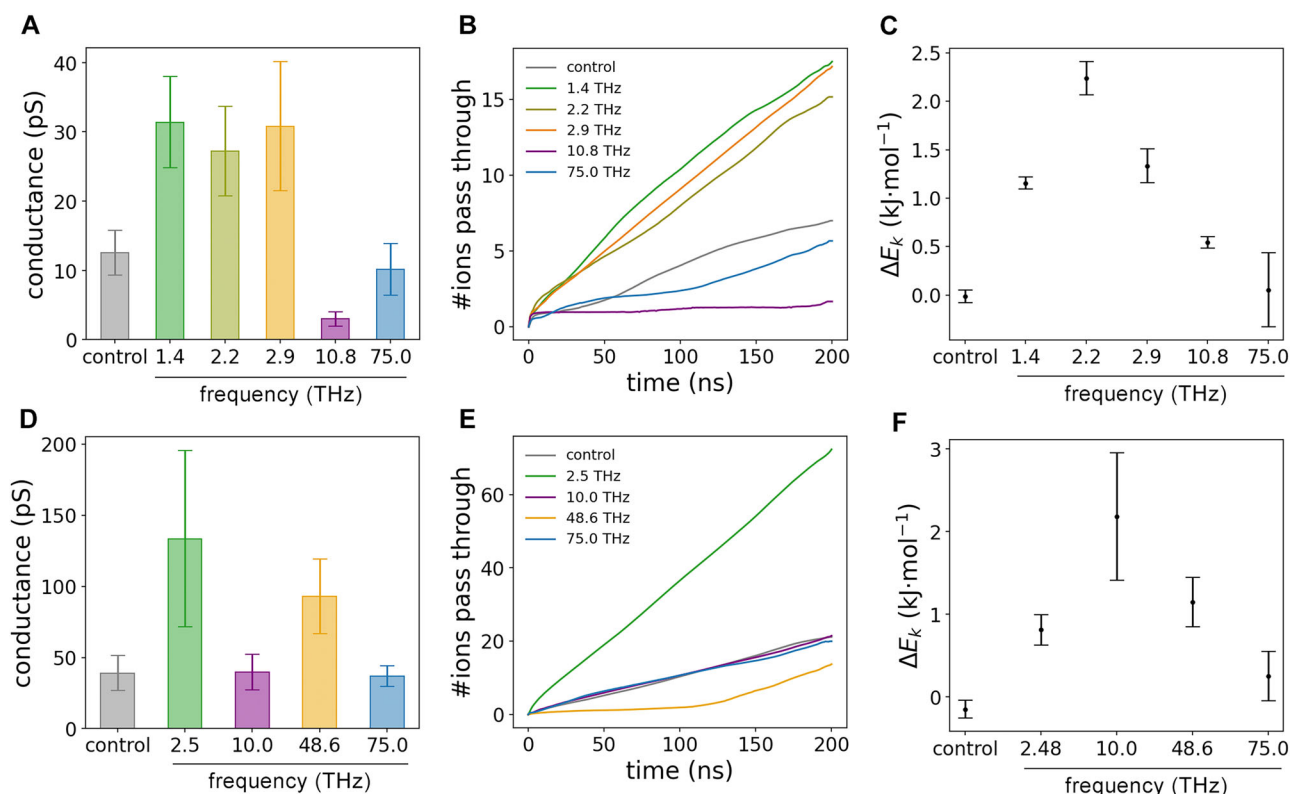


**Fig. 3 | The effect of THz field on ion permeation.** (A, D) The effect of THz electromagnetic fields at different frequencies on the ion permeation of  $K_v1.2$  (A) and  $Na_v1.5$  (D). (B, E) The time-resolved average number of ions permeating

through  $K_v1.2$  (B) and  $Na_v1.5$  (E). The curves were smoothed by taking the sliding average in 2 ns intervals. (C, F)  $\Delta E_k$  of ions at the SF of  $K_v1.2$  (C) and  $Na_v1.5$  (F) when different THz fields were applied.



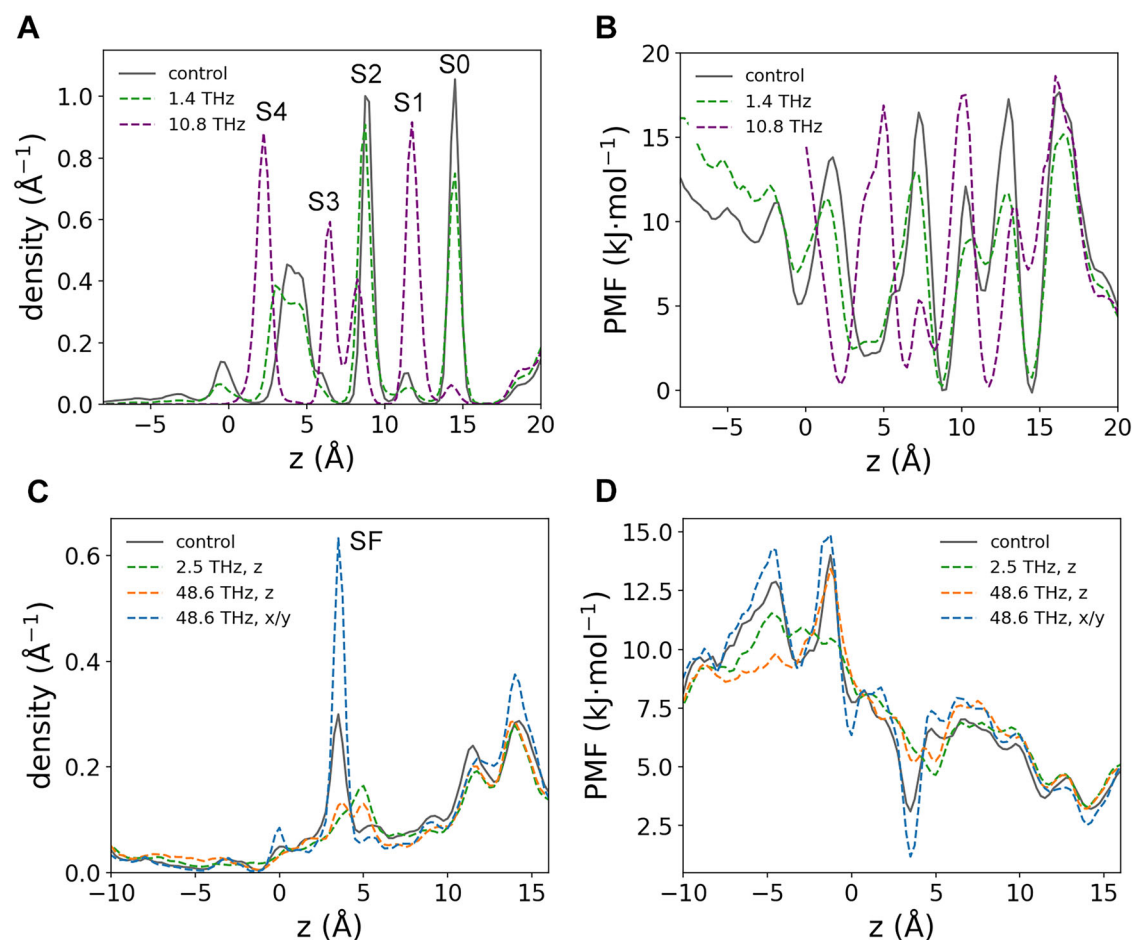


**Fig. 4 | The effect of THz field on ion distribution and PMF.** (A, B) The distribution and PMF of  $K^+$  along the z-axis within  $K_v1.2$ . (C, D) The distribution and PMF of  $Na^+$  within  $Na_v1.5$ .

**The free energy barrier was reduced when THz field enhanced ion permeation.** Previous works discovered that THz field can alter the distribution and free energy profile of ions, which can possibly affect the ion permeability<sup>6,15</sup>. Here, we computed the ion distribution and PMF to identify whether the above THz field can enhance ion permeation by altering the energy profile.

When the 1.4 THz field was applied to the  $K_v1.2$  channel, no significant differences in ion distribution were observed, indicating that the binding sites remained unchanged (Fig. 4A). Meanwhile, the energy barriers between the binding sites, defined as the difference between peaks and troughs in the PMF curve, was reduced (Fig. 4B). The largest energy barrier, through which an ion at S0 escapes to the solution, was reduced from 17.8 kJ/mol to 14.4 kJ/mol. Similar results were observed when 2.5 and 48.6 THz fields were applied to  $Na_v1.5$ . The ion density in the SF was lower, and the energy barrier decreased from 10.9 kJ/mol to 6.9 and 8.2 kJ/mol respectively (Fig. 4C, D). As a result, the ions can overcome the energy barrier easier and permeate faster.

**THz field reduced hydrogen bonds between protein and water.** Furthermore, we calculated the number of hydrogen bonds between the protein and water with the focus of hydrogen bonds formed by SF. For both  $K_v1.2$  and  $Na_v1.5$ , the number of hydrogen bonds slightly decreased when THz fields were applied. In  $K_v1.2$ , the average number of hydrogen bonds formed between protein and water decreased from 298 to 290 in the presence of a 1.4 THz field, and decreased to 279 when a 10.8 THz field was applied (Figure S4 A). The number of hydrogen bonds between SF and water also decreased from 7.2 to 5.9 and 3.9, mainly affecting the hydroxyl group of residue Thr370 (Figure S4 B). For

$Na_v1.5$ , the average number of hydrogen bonds between protein and water decreased from 538 to 504 and 490 when a 2.5 THz or 48.6 THz field was applied (Figure S4 C). The number of hydrogen bonds between SF and water also decreased from 23 to 19 and 18, respectively, mainly resulted from fewer hydrogen bonds at the carboxyl groups in SF (Figure S4 D). This agrees with previous findings that the THz field can destabilize hydrogen bonds formed by the channel and water<sup>15,16</sup>, although this effect does not necessarily concur with an increase in ion permeability.

### Simulations under non-specific conditions

**The effect of non-specific frequencies.** To assess whether the observed effects were specific to the peak frequencies, we performed additional simulations using non-specific frequencies. For this purpose, we chose a 75.0 THz field, which was distant from the peak frequencies identified in our spectrum and thus less likely to cause interference.

No significant changes in ion permeation were observed when a 75.0 THz field was applied to each channel. The conductance values for  $K_v1.2$  and  $Na_v1.5$  were  $10.2 \pm 3.7$  pS and  $36.9 \pm 7.4$  pS, respectively (Fig. 3A, D). These values were consistent with the control measurements, suggesting that the changes in ion permeation observed in the above sections were specific to those selected frequencies and not due to a general effect of the THz field. Additionally, no significant changes in  $\Delta E_k$  was observed, although the perturbation induced a larger fluctuation in  $\Delta E_k$  (Fig. 3C, F). Therefore, this control experiment reinforces the idea that the peak frequencies identified by FFT analyses have a specific effect on ion channels, rather than simply causing a general perturbation.

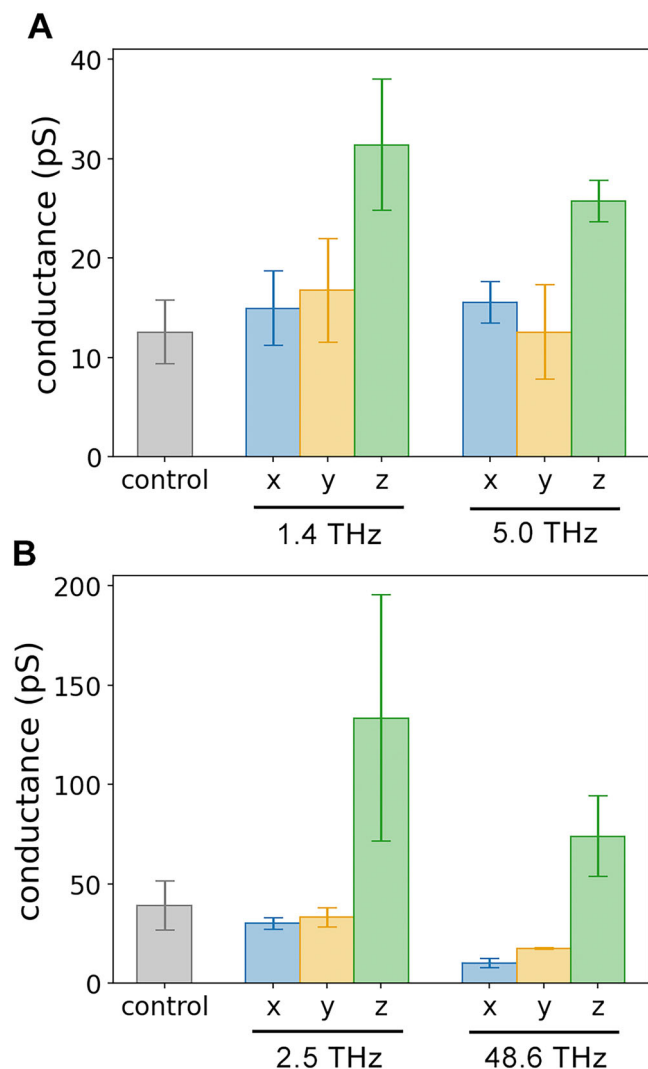


**Fig. 5 | The effect of THz field in different directions.** The effect of THz field in different directions on the ion permeation of (A) K<sub>v</sub>1.2 and (B) Na<sub>v</sub>1.5.

**The effect of THz field in different directions.** We further investigated the specificity of the THz field's polarization direction on its effects by conducting simulations with the THz field applied in the x and y directions, in addition to the z direction.

For K<sub>v</sub>1.2, a 1.4 THz field significantly affected ion permeation when polarized in the z direction but had negligible effects when applied in the x or y directions. Furthermore, although potassium ions showed a peak frequency of 5.0 THz in the x-y plane, applying an electric field at this frequency in the x or y directions did not significantly impact ion permeation. In contrast, applying the 5.0 THz field in the z direction increased ion conductance to  $25.7 \pm 2.1$  pS ( $n = 3$ ,  $p < 0.01$ ), probably due to its proximity to the peak frequencies in the z direction (Fig. 5A). This increase was less pronounced than that observed with the peak frequencies, further supporting the frequency specificity of THz fields.

Similarly, in the case of Na<sub>v</sub>1.5, applying a 2.5 THz field along the x or y direction did not result in significant changes in ion permeation. Interestingly, when a 48.6 THz field was applied in the x or y direction, the conductance notably decreased to  $10.1 \pm 3.1$  pS and  $17.5 \pm 2.3$  pS, respectively ( $n = 6$  each,  $p < 0.05$ ) (Fig. 5B). This decrease was accompanied by an increase in ion density and energy barrier at the SF (Fig. 4C, D), indicating a tighter binding of Na<sup>+</sup> ions to the SF of the channel, which likely caused the reduced ion permeability. These observations indicate that the influence of the THz field on ion channels is indeed specific to its polarization direction.

### The effect of THz field with different amplitudes

We further investigated the effect of THz field amplitude by conducting simulations with varying amplitudes. For K<sub>v</sub>1.2, we applied a 1.4 THz electromagnetic field, while for Na<sub>v</sub>1.5, a 2.5 THz field was used. The amplitudes tested were 0.2, 0.4, 0.6 and 0.8 V/nm.

Both K<sub>v</sub>1.2 and Na<sub>v</sub>1.5 showed a positive correlation between the field amplitude and ion permeation. The conductance of K<sub>v</sub>1.2 increased at all three amplitudes, with a linear relationship between amplitude and ion permeation, evidenced by a correlation coefficient of 0.84 (Fig. 6A). Na<sub>v</sub>1.5 showed a similar but slightly different response. The conductance only increased insignificantly when the amplitude was 0.2 or 0.4 V/nm, while a greater enhancement in ion permeability occurred at the amplitude of 0.6 or 0.8 V/nm. This indicates a non-linear relationship between the THz field amplitude and the ion permeability, suggesting that a higher amplitude is required to significantly influence the ion permeability of Na<sub>v</sub>1.5 (Fig. 6D).

$\Delta E_k$  also exhibited a positive correlation with the amplitude for both K<sub>v</sub>1.2 and Na<sub>v</sub>1.5 (Fig. 6B, E). This shows that as the amplitude of the THz field increased, the vibrational motion of the ions was stimulated to a higher extent, thus increasing the kinetic energy. We also noticed that  $\Delta E_k$  was not proportional to increase in conductance, and a different nonlinear effect appeared between K<sub>v</sub>1.2 and Na<sub>v</sub>1.5, which could be due to differences in their structures.

The residence time of the ions within the channels adopted a negative correlation with the THz field amplitude, further confirming that the THz field influences ion motion and accelerates permeation (Fig. 6C, F). The residence time of K<sup>+</sup> in K<sub>v</sub>1.2 reduced from  $63 \pm 10$  ns to  $29 \pm 6$  ns, roughly halved when the amplitude increased to 0.8 V/nm. The residence time of Na<sup>+</sup> in Na<sub>v</sub>1.5 experienced a greater decrease from  $3.6 \pm 0.4$  ns to  $0.7 \pm 0.1$  ns, about one fifth of the original value.

The ion density and PMF also exhibited a gradual change (Figure S5). In K<sub>v</sub>1.2, the PMF peaks at  $z = 1.7, 7.2, 13.0, 16.2$  Å decreased, and in Na<sub>v</sub>1.5, the PMF peak at  $z = -1.2$  Å decreased and the well at  $z = 3.5$  Å increased. Both resulted in a lower energy barrier and therefore facilitated ion permeability.

### Discussion

Despite numerous experimental and computational studies on the effects of THz fields on ion channels, it remained unclear at the molecular level whether the observed effects were specific or simply due to thermal influence. In our simulations, the system temperature was consistently maintained at 310 K with a high thermal coupling rate. No significant temperature changes were observed, with fluctuations of only 1.75 K in the K<sub>v</sub>1.2 system and 1.35 K in the Na<sub>v</sub>1.5 system. Moreover, if the effects of the THz field were purely thermal, they would not exhibit directional specificity. However, our simulations demonstrated that the THz field effects were both frequency- and direction-specific. Therefore, the observed changes in conductance in our simulations can be attributed to the non-thermal effects of the THz electromagnetic fields.

Our study demonstrates that the influence of THz electromagnetic fields on ion channels is highly specific to both frequency and polarization direction. THz fields resonating at the frequencies of potassium ions within K<sub>v</sub>1.2 (1.4, 2.2, and 2.9 THz) and sodium ions within Na<sub>v</sub>1.5 (2.5 THz) directly enhance ion permeation by accelerating ion motion along the permeating direction (z-axis). In contrast, a 10.8 THz field, resonating with the carbonyl oxygen atoms of the selectivity filter, alters ion distribution within K<sub>v</sub>1.2, resulting in decreased ion permeability. These findings suggest that ion permeation through ion channels can be modulated by THz electromagnetic fields through multiple mechanisms, underscoring a multifaceted approach to controlling molecular behavior. While most of the previous research focused on frequencies associated with the protein motions, which influence ion motion indirectly, our study also revealed frequencies that resonate directly with the permeating ions at the SF, yielding more pronounced effects. Interestingly, a very recent study on the open-state model of the KcsA channel discovered a characteristic peak of

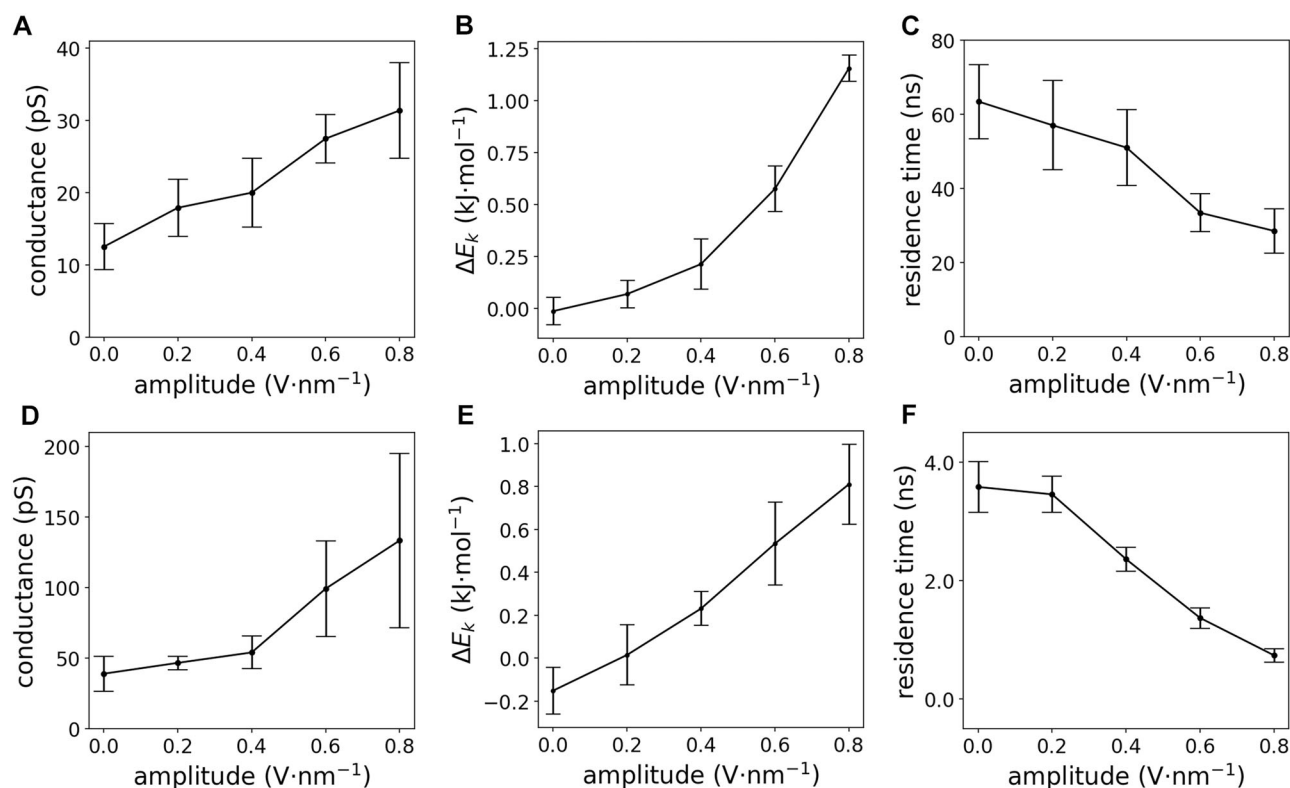


**Fig. 6 | The effect of THz field with different amplitudes.** Relationship between THz field amplitude and ion permeation,  $\Delta E_k$ , and residence time of K<sub>v</sub>1.2 (A–C) and Na<sub>v</sub>1.5 (D–F).

ion vibration parallel to the channel axis located at 2.4 THz<sup>49</sup>, which is very close to one of the peaks we found for K<sub>v</sub>1.2.

Given the similar structure of other ion channels in the K<sub>v</sub> and Na<sub>v</sub> families, we believe that our results can be generalized to other K<sub>v</sub> and Na<sub>v</sub> channels. However, some key differences can be observed between the K<sub>v</sub> and Na<sub>v</sub> channels. The K<sup>+</sup> and Na<sup>+</sup> ions exhibited close but distinct characteristic frequencies in the K<sub>v</sub> and Na<sub>v</sub> channels, which resulted from the different structures of the SF and the different energy profiles of the ions. The two channels also differ in their responses to the amplitude of THz fields. The reason may be that K<sub>v</sub> channels have more well-defined ion binding sites than Na<sub>v</sub> channels, which makes resonance vibration of K<sup>+</sup> in the K<sub>v</sub> channels more likely to occur than Na<sup>+</sup> in the Na<sub>v</sub> channels.

Our study demonstrates that ion channel function can be modulated by specific THz fields, opening new avenues for applications in biomedical fields, particularly in the treatment of channelopathies. The non-invasive and non-destructive nature of THz waves, combined with their ability to be precisely directed and focused, presents a promising therapeutic modality. Moreover, this approach could be extended to identify specific frequencies that affect other biomolecules, offering a versatile tool for molecular manipulation.

Despite these promising findings, our study has some limitations. The simulated electric field amplitude of 0.8 V/nm is significantly higher than what might be safely applied in practical scenarios, and the simulation duration may not fully capture the effects over longer periods. Therefore, further experimental studies are essential to validate the impact of THz fields on ion channels and their effects on cellular behavior at the macroscopic level. These future investigations should focus on refining the intensity and duration of exposure to ensure both safety and efficacy in real-world applications.

## Methods

### Model systems

The K<sub>v</sub>1.2 model was built with the open-state structure of a chimeric protein K<sub>v</sub>1.2/2.1 (PDB: 2R9R). Constructed from rat K<sub>v</sub>1.2 and K<sub>v</sub>2.1, this

protein has an identical pore region as K<sub>v</sub>1.2, and produces a similar current to K<sub>v</sub>1.2<sup>29</sup>. The pore region (residues 309 ~ 417 of each subunit) and the K<sup>+</sup> within were selected and embedded in 1-palmitoyl-2-oleoyl-glycero-3-phosphocholine (POPC) bilayer to mimic the cellular membrane environment. The system was solvated with an aqueous solution containing 150 mM KCl. The channel axis was orientationed along the z axis, and the membrane parallel to the x-y plane. The TIP3P model was used for water molecules. The simulation system was prepared using CHARMM-GUI<sup>50</sup>. The final system size was 7.66 × 7.66 × 8.26 nm<sup>3</sup>, containing 34 K<sup>+</sup>, 22 Cl<sup>-</sup>, 128 POPC and 8716 water molecules.

The Na<sub>v</sub>1.5 model was built likewise using the open-state structure with 4 *IT*-helices, constructed by Choudhury et al.<sup>45</sup>. The pore region (residues 236 ~ 430, 825 ~ 945, 1320 ~ 1478, 1643 ~ 1777) was selected and embedded in a POPC bilayer. The system was solvated in a solution containing 150 mM NaCl. The final system size was 8.33 × 8.33 × 10.84 nm<sup>3</sup>, containing 57 Na<sup>+</sup>, 42 Cl<sup>-</sup>, 147 POPC and 15907 water molecules.

### MD simulations

We performed molecular dynamics (MD) simulations using GROMACS 2022.3<sup>51</sup>, augmented with an in-house developed plugin that enabled the addition of a constant electric field in each spatial direction (x, y, or z). This capability allowed us to simulate ion permeation in the presence of both an oscillating electric field and a uniform electric field along the channel axis.

The simulations were conducted under various conditions (Table 1), each with 3 ~ 6 replicates. The control and specific conditions were simulated with six replicates, while non-specific conditions were repeated three times. A total of 24  $\mu$ s simulation was performed in this study.

The CHARMM36m force field<sup>52,53</sup> and periodic boundary condition (PBC) were employed for the simulation. Leap-frog algorithm was used with a 2 fs time step. Temperature was maintained at 310 K using the Nose-Hoover thermostat<sup>54</sup>, and pressure was kept constant at 1 atm using the C-rescale barostat<sup>55</sup>. Particle-Mesh Ewald (PME) was used for long-range electrostatic calculations<sup>56</sup>. Van der Waals forces were considered up to a

**Table 1 | Simulation systems, conditions, and replicates**

System	Frequency [THz]	Direction	Amplitude [V nm <sup>-1</sup> ]	Time [ns]	Replicates
K <sub>v</sub> 1.2	–	–	–	200	6
	1.4	x	0.8	200	3
	1.4	y	0.8	200	3
	1.4	z	0.2	200	6
	1.4	z	0.4	200	6
	1.4	z	0.6	200	6
	1.4	z	0.8	200	6
	2.2	z	0.8	200	6
	2.9	z	0.8	200	6
	5.0	x	0.8	200	3
	5.0	y	0.8	200	3
	5.0	z	0.8	200	3
Na <sub>v</sub> 1.5	10.8	z	0.8	200	3
	75.0	z	0.8	200	3
	–	–	–	200	6
	2.5	x	0.8	200	3
	2.5	y	0.8	200	3
	2.5	z	0.2	200	6
	2.5	z	0.4	200	6
	2.5	z	0.6	200	6
	2.5	z	0.8	200	6
	10.0	z	0.8	200	6
	48.6	x	0.8	200	6
	48.6	y	0.8	200	6
	48.6	z	0.8	600	4
	75.0	z	0.8	200	3

cutoff of 1.2 nm, with a switching function applied from 1.0 nm to smooth the transition.

To maintain the open state of the channels, a position restraint of 100 kJ/(mol · nm<sup>2</sup>) was applied to the protein backbone, except for the selectivity filter region (residues 370 ~ 375 for K<sub>v</sub>1.2, and residues 372 ~ 376, 900 ~ 904, 1420 ~ 1425, 1712 ~ 1716 for Na<sub>v</sub>1.5). A constant electric field  $E_0$  was applied along z direction to establish a +450 or –450 mV transmembrane potential, calculated as the product of  $E_0$  and the length of the box along z direction  $l_z$ <sup>32</sup>

$$U = E_0 l_z$$

The ratio of electric field to magnetic field in electromagnetic waves equals the light speed  $c$ . Given that the velocities of charged particles in the system are far lower than  $c$ , the impact of the magnetic component is negligible<sup>6</sup>. Consequently, only the electric component was considered in our simulations. The total electric field applied to the system was therefore

$$\mathbf{E}(t) = \mathbf{E}_0 + \mathbf{A} \cos(2\pi ft)$$

Where  $A$  and  $f$  denote the amplitude and frequency of the THz field.

### Trajectory and frequency analysis

All trajectory analysis were performed utilizing MDAnalysis 2.7.0 package in Python 3.11. After the equilibration of each system, a 1-ns simulation was performed for the frequency analysis. The same simulation setup was adopted as above, except that no restraints or electric field were applied. The 1 ns trajectory was split into 20 intervals. For each interval, FFT was

performed on the velocities of ions and atom groups using NumPy 1.25.2. The modulus of Fourier coefficients were averaged among all intervals to obtain their frequency spectra. The frequency spectra of bonds, angles and dihedrals are calculated likewise. The formula of FFT can be written as

$$A(k) = \sum_t f(t) e^{-2\pi i k t}$$

Where  $f(t)$  can be the velocities in each dimension, bond lengths, angles or dihedral angles.

The modulus of the Fourier coefficients in x, y, and z dimensions indicates the vibrational mode for a certain frequency. For example, if the coefficient in z direction is much greater than in x, y directions, this vibrational mode mainly occurs along z axis.

### Calculation of conductance

The conductance of a channel was calculated from the number of ions passing through in the simulation time under the transmembrane potential<sup>45,57</sup>:

$$G = \frac{I}{U} = \frac{Nq}{Ut}$$

Where  $N$  is the number of ions passing through in time  $t$ ,  $I$  and  $U$  denote the current and transmembrane potential, and  $q$  is the charge of each ion.

### Calculation of PMF

The PMF was calculated from the logarithm of the ion density<sup>15,32,47,57</sup>:

$$E(z) = -kT \ln \rho(z)$$

where  $k$  and  $T$  are the Boltzmann constant and the temperature, and  $\rho(z)$  denotes the ion density inside the channel along the z-axis. Please note that, as our simulations were conducted under non-equilibrium conditions, the PMF should be considered as Pseudo-PMF.

### Data availability

The initial and final configurations of the MD simulation are available in Supplemental Data. All other data are available upon reasonable request.

### Code availability

The MD plugin is available on GitHub ([https://github.com/ComputBiophys/GMX\\_ElectricField\\_Plugin](https://github.com/ComputBiophys/GMX_ElectricField_Plugin)).

Received: 23 September 2024; Accepted: 24 March 2025;

Published online: 03 April 2025

### References

- Lehmann-Horn, F. & Jurkat-Rott, K. Voltage-gated ion channels and hereditary disease. *Physiol. Rev.* **79**, 1317–1372 (1999).
- Resta, C. D. & Becchetti, A. *Integrins and Ion channels: Molecular Complexes and Signaling* (Landes Bioscience and Springer Science +Business Media, 2010).
- Bezanilla, F. Voltage-gated ion channels. *IEEE Trans. Nano Biosci.* **4**, 34–48 (2005).
- Armstrong, C. M. Voltage-gated K channels. *Science's STKE* **2003**, re10 (2003).
- Roux, B. Ion channels and ion selectivity. *Essays Biochem.* **61**, 201–209 (2017).
- Li, Y., Chang, C., Zhu, Z., Sun, L. & Fan, C. Terahertz wave enhances permeability of the voltage-gated calcium channel. *J. Am. Chem. Soc.* **143**, 4311–4318 (2021).
- Liu, X. et al. Nonthermal and reversible control of neuronal signaling and behavior by midinfrared stimulation. *Proc. Natl. Acad. Sci. USA* **118**, e2015685118 (2021).



8. Sun, Y. et al. A non-invasive and DNA-free approach to upregulate mammalian voltage-gated calcium channels and neuronal calcium signaling via terahertz stimulation. *Adv. Sci.* **11**, 2405436 (2024).
9. Tan, X. et al. Minimal-invasive enhancement of auditory perception by terahertz wave modulation. *Nano Res.* **15**, 5235–5244 (2022).
10. Wang, Y. et al. Regulation of ion permeation of the KcsA channel by applied midinfrared field. *Int. J. Mol. Sci.* **24**, 556 (2022).
11. Wang, Y. et al. Effect of thz waves of different orientations on  $K^+$  permeation efficiency in the kcsa channel. *Int. J. Mol. Sci.* **25**, 429 (2023).
12. Wu, K. et al. Enhancement of  $K^+$  channel permeation by selective terahertz excitation. *Spectrochim. Acta Pt. A: Mol. Biomol. Spectrosc.* **305**, 123538 (2024).
13. Zhao, Y., Wang, L., Li, Y. & Zhu, Z. Terahertz waves enhance the permeability of sodium channels. *Symmetry*. **15**, 427 (2023).
14. Zhao, X. et al. Structural insights and influence of terahertz waves in midinfrared region on Kv1.2 channel selectivity filter. *ACS Omega* **9**, 9702–9713 (2024).
15. Ding, W. et al. Effect of terahertz electromagnetic field on the permeability of potassium channel Kv1.2. *Int. J. Mol. Sci.* **24**, 10271 (2023).
16. Zhao, X. et al. Permeability enhancement of Kv1.2 potassium channel by a terahertz electromagnetic field. *J. Chem. Phys.* **159**, 045101 (2023).
17. Hu, Z.-H., Lv, W.-P., Hui, D.-X., Wang, X.-J. & Wang, Y.-N. Permeability enhancement of the KcsA channel under radiation of a terahertz wave. *Phys. Rev. E* **105**, 024104 (2022).
18. Guo, L., Bo, W., Wang, K., Wang, S. & Gong, Y. Theoretical investigation on the effect of terahertz wave on  $Ca^{2+}$  transport in the calcium channel. *iScience* **25**, 103561 (2022).
19. Zhu, Z. et al. Tunable surface wettability via terahertz electrowave controlled vicinal subnanoscale water layer. *Nano Lett.* **24**, 3243–3248 (2024).
20. Zhang, Q. L. et al. Ultrahigh-flux water nanopumps generated by asymmetric terahertz absorption. *Phys. Rev. Lett.* **132**, 184003 (2024).
21. Alexandrov, B. S. et al. Specificity and heterogeneity of terahertz radiation effect on gene expression in mouse mesenchymal stem cells. *Sci. Rep.* **3**, 1184 (2013).
22. Nikitkina, A. I. et al. Terahertz radiation and the skin: a review. *J. Biomed. Opt.* **26**, 043005 (2021).
23. Li, D. et al. Detecting melanoma with a terahertz spectroscopy imaging technique. *Spectrochim. Acta Pt. A: Mol. Biomol. Spectrosc.* **234**, 118229 (2020).
24. Li, Y. et al. Physicochemical insights on terahertz wave diminished side effects of drugs from slow dissociation. *ACS Nano* **16**, 8419–8426 (2022).
25. Gutman, G. A. et al. International union of pharmacology. LIII. nomenclature and molecular relationships of voltage-gated potassium channels. *Pharmacol. Rev.* **57**, 473–508 (2005).
26. Sands, Z., Grottesi, A. & Sansom, M. S. Voltage-gated ion channels. *Curr. Biol.* **15**, R44–7 (2005).
27. Ong, S. T., Tyagi, A., Chandy, K. G. & Bhushan, S. Mechanisms underlying C-type inactivation in Kv channels: Lessons from structures of human Kv1.3 and fly Shaker-IR channels. *Front. Pharmacol.* **13**, 924289 (2022).
28. Ye, W. et al. Activation and closed-state inactivation mechanisms of the human voltage-gated  $K_v4$  channel complexes. *Mol. Cell* **82**, 2427–2442 (2022).
29. Long, S. B., Tao, X., Campbell, E. B. & MacKinnon, R. Atomic structure of a voltage-dependent  $K^+$  channel in a lipid membrane-like environment. *Nature* **450**, 376–82 (2007).
30. Jensen, M. O. et al. Principles of conduction and hydrophobic gating in  $K^+$  channels. *Proc. Natl. Acad. Sci. USA* **107**, 5833–5838 (2010).
31. Jensen, M. O. et al. Mechanism of voltage gating in potassium channels. *Science* **336**, 229–233 (2012).
32. Jensen, M. O., Jogini, V., Eastwood, M. P. & Shaw, D. E. Atomic-level simulation of current-voltage relationships in single-file ion channels. *J. Gen. Physiol.* **141**, 619–32 (2013).
33. Reddi, R., Matulef, K., Riederer, E. A., Whorton, M. R. & Valiyaveetil, F. I. Structural basis for C-type inactivation in a Shaker family voltage-gated  $K^+$  channel. *Sci. Adv.* **8**, eabm8804 (2022).
34. Catterall, W. A., Goldin, A. L. & Waxman, S. G. International union of pharmacology. XLVII. nomenclature and structure-function relationships of voltage-gated sodium channels. *Pharmacol. Rev.* **57**, 397–409 (2005).
35. Catterall, W. A., Lenaues, M. J. & Gamal El-Din, T. M. Structure and pharmacology of voltage-gated sodium and calcium channels. *Annu. Rev. Pharmacol. Toxicol.* **60**, 133–154 (2020).
36. Nau, C. Voltage-gated ion channels. *Handb. Exp. Pharmacol.* **182**, 85–92 (2008).
37. Kwong, K. & Carr, M. J. Voltage-gated sodium channels. *Curr. Opin. Pharm.* **22**, 131–9 (2015).
38. Ing, C. & Pomes, R. Simulation studies of ion permeation and selectivity in voltage-gated sodium channels. *Curr. Top. Membr.* **78**, 215–60 (2016).
39. Li, Y. & Gong, H. Theoretical and simulation studies on voltage-gated sodium channels. *Protein Cell* **6**, 413–22 (2015).
40. Flood, E., Boiteux, C. & Allen, T. W. Selective ion permeation involves complexation with carboxylates and lysine in a model human sodium channel. *PLoS Comp. Biol.* **14**, e1006398 (2018).
41. Jiang, D. et al. Open-state structure and pore gating mechanism of the cardiac sodium channel. *Cell* **184**, 5151–5162 (2021).
42. Alberini, G. et al. Molecular dynamics simulations of ion permeation in human voltage-gated sodium channels. *J. Chem. Theory Comput.* **19**, 2953–2972 (2023).
43. Rook, M. B., Evers, M. M., Vos, M. A. & Bierhuizen, M. F. Biology of cardiac sodium channel  $Na_v1.5$  expression. *Cardiovasc. Res.* **93**, 12–23 (2012).
44. Veerman, C. C., Wilde, A. A. & Lodder, E. M. The cardiac sodium channel gene *SCN5A* and its gene product  $Na_v1.5$ : Role in physiology and pathophysiology. *Gene* **573**, 177–87 (2015).
45. Choudhury, K. & Delemotte, L. Modulation of pore opening of eukaryotic sodium channels by  $\pi$ -helices in S6. *J. Phys. Chem. Lett.* **14**, 5876–5881 (2023).
46. Smart, O. S., Neduvellil, J. G., Wang, X., Wallace, B. & Sansom, M. S. HOLE: A program for the analysis of the pore dimensions of ion channel structural models. *J. Mol. Graph.* **14**, 354–360 (1996).
47. Zhu, Z. et al. Design of artificial biomimetic channels with  $Na^+$  permeation rate and selectivity potentially outperforming the natural sodium channel. *Nano Res.* **17**, 8638–8646 (2024).
48. Weiss, R. E. & Horn, R. Functional differences between two classes of sodium channels in developing rat skeletal muscle. *Science* **233**, 361–364 (1986).
49. Wang, Y. et al. A physical derivation of high-flux ion transport in biological channel via quantum ion coherence. *Nat. Commun.* **15**, 7189 (2024).
50. Lee, J. et al. CHARMM-GUI input generator for NAMD, GROMACS, AMBER, OpenMM, and CHARMM/OpenMM simulations using the CHARMM36 additive force field. *J. Chem. Theory Comput.* **12**, 405–413 (2016).
51. Abraham, M. J. et al. GROMACS: High performance molecular simulations through multi-level parallelism from laptops to supercomputers. *SoftwareX* **1–2**, 19–25 (2015).
52. Vanommeslaeghe, K. et al. CHARMM general force field: A force field for drug-like molecules compatible with the CHARMM all-atom additive biological force fields. *J. Comput. Chem.* **31**, 671–90 (2010).
53. Huang, J. et al. CHARMM36m: an improved force field for folded and intrinsically disordered proteins. *Nat. Methods* **14**, 71–73 (2017).
54. Hoover, W. G. Canonical dynamics: Equilibrium phase-space distributions. *Phys. Rev. A* **31**, 1695–1697 (1985).

55. Bernetti, M. & Bussi, G. Pressure control using stochastic cell rescaling. *J. Chem. Phys.* **153**, 114107 (2020).
56. Essmann, U. et al. A smooth particle mesh Ewald method. *J. Chem. Phys.* **103**, 8577–8593 (1995).
57. Wilson, M. A., Wei, C., Bjelkmar, P., Wallace, B. A. & Pohorille, A. Molecular dynamics simulation of the antiameobin ion channel: linking structure and conductance. *Biophys. J.* **100**, 2394–402 (2011).

## Acknowledgements

This work was supported by the Science Fund for Creative Research Groups of the National Natural Science Foundation of China (T2321001). The MD simulations were performed on the computing platform of the Center for Life Sciences at Peking University and the National Supercomputer Center in Tianjin.

## Author contributions

Conceptualization: C.S., Q.O., Methodology and Investigation: Z.S., L.X., Supervision: C.S., Q.O., Writing: Z.S., L.X., C.S.

## Competing interests

The authors declare no competing interests.

## Additional information

**Supplementary information** The online version contains supplementary material available at <https://doi.org/10.1038/s42004-025-01503-4>.

**Correspondence** and requests for materials should be addressed to Chen Song.

**Peer review information** *Communications Chemistry* thanks Zhi Zhu, Chao Chang, and the other, anonymous, reviewer for their contribution to the peer review of this work.

**Reprints and permissions information** is available at <http://www.nature.com/reprints>

**Publisher's note** Springer Nature remains neutral with regard to jurisdictional claims in published maps and institutional affiliations.

**Open Access** This article is licensed under a Creative Commons Attribution-NonCommercial-NoDerivatives 4.0 International License, which permits any non-commercial use, sharing, distribution and reproduction in any medium or format, as long as you give appropriate credit to the original author(s) and the source, provide a link to the Creative Commons licence, and indicate if you modified the licensed material. You do not have permission under this licence to share adapted material derived from this article or parts of it. The images or other third party material in this article are included in the article's Creative Commons licence, unless indicated otherwise in a credit line to the material. If material is not included in the article's Creative Commons licence and your intended use is not permitted by statutory regulation or exceeds the permitted use, you will need to obtain permission directly from the copyright holder. To view a copy of this licence, visit <http://creativecommons.org/licenses/by-nc-nd/4.0/>.

© The Author(s) 2025